Investigation on the Effect of Sulfur and Titanium on the Microstructure of Lamellar Graphite Iron

ELHAM MOUMENI, DORU MICHAEL STEFANESCU, NIELS SKAT TIEDJE,
PELLO LARRAÑAGA, and JESPER HENRI HATTEL

The goal of this work was to identify the inclusions in lamellar graphite cast iron in an effort to explain the nucleation of the phases of interest. Four samples of approximately the same carbon equivalent but different levels of sulfur and titanium were studied. The Ti/S ratios were from 0.15 to 29.2 and the Mn/S ratios from 4.2 to 48.3. Light and electron microscopy were used to examine the unetched, color-etched, and deep-etched samples. It was confirmed that in irons with high sulfur content (0.12 wt pct) nucleation of type-A and type-D graphite occurs on Mn sulfides that have a core of complex Al, Ca, Mg oxide. An increased titanium level of 0.35 pct produced superfine interdendritic graphite (~10 μm) at low (0.012 wt pct) as well as at high-S contents. Ti also caused increased segregation in the microstructure of the analyzed irons and larger eutectic grains (cells). TiC did not appear to be a nucleation site for the primary austenite as it was found mostly at the periphery of the secondary arms of the austenite, in the last region to solidify. The effect of titanium in refining the graphite and increasing the austenite fraction can be explained through the widening of the liquidus-eutectic temperature interval (more time for austenite growth) and the decrease in the growth rate of the graphite because of Ti absorption on the graphite. The fact that Ti addition produced larger eutectic cells supports the theory that Ti is not producing finer graphite because of a change in the nucleation potential, but because of lower growth rate of the graphite in between the dendrite arms of a larger fraction of austenite. In the presence of high-Ti and S, (MnTi)S star-like and rib-like inclusions precipitate and act as nuclei for the austenite.

I. INTRODUCTION

THE main solidification parameters affecting the mechanical properties of hypoeutectic gray (lamellar graphite) irons include the fraction of primary austenite and the shape, size, and distribution of graphite. In foundry practice they are controlled through the chemical composition (carbon equivalent and alloying elements) and inoculation. Recently, using appropriate titanium additions in a low sulfur 4 pct carbon equivalent gray iron Larrañaga et al.[1] increased significantly the austenite fraction. This was accompanied by the solidification of, what they termed, superfine lamellar interdendritic graphite, which was associated with high tensile strength of 300 to 350 MPa, without a significant increase in hardness, which remained in the range of 185 to 200 HB.[2] The superfine graphite is short (10 to 20 μm) and stubby. Thermal analysis on standard cooling curve cups and keel blocks indicated an increase of the liquidus temperature with titanium, suggesting an austenite nucleation effect. The eutectic temperature decreased. Overall the liquidus/eutectic temperature interval significantly increased. This was interpreted as increased time for austenite solidification, which explains the increase in the austenite fraction. While the various inclusions were not positively identified, it was state that Ti compounds that were found mostly in the matrix did not appear to act as graphite nuclei. Manganese sulfides were found mostly in the proximity of the graphite, which qualifies them for possible graphite nuclei.

It is well known that a number of pure metals such as Li, Ca, Ba[3], Sr, and Na[4] can be effective in promoting graphite nucleation in cast iron. All these metals are strong oxide and sulfide formers. Their use as pure metals for inoculation purposes is impractical. Attempting to explain the efficiency of metals such as Ca, Ba, Sr, Na in the inoculation of lamellar graphite iron, Lux[5] suggested that these, and all elements from groups I, II, and III from the periodic table, when introduced in molten iron, form salt-like carbides that develop epitaxial planes with the graphite, and thus constitute nuclei for graphite.

Later, Weis[6] assumed that nucleation of lamellar graphite occurs on SiO$_2$ oxides formed by heterogeneous

ELHAM MOUMENI, Ph.D. Student, NIELS SKAT TIEDJE, Associate Professor, and JESPER HENRI HATTEL, Professor, are with the Technical University of Denmark, Kongens Lyngby, Denmark. DORU MICHAEL STEFANESCU, Professor Emeritus, is with The Ohio State University, Columbus, OH, and also with The University of Alabama, Tuscaloosa, AL. Contact e-mail: stefanescu.1@osu.edu PELLO LARRAÑAGA, Project Leader, is with the IK4-Azterlan Metallurgical Centre, 48200 Durango, Spain.

catalysis of CaO, Al_2O_3, and oxides of other alkaline metals. At about the same time the role of MnS in graphite nucleation was implied through experiments based on thermal analysis of cast iron.[7] A MnS ratio of 12.3 was found to produce the lowest eutectic undercooling. Note that this is way in excess of the stoichiometric ratio Mn/S = 1.7. Eventually, a consensus was reached that graphite flakes nucleate on MnS or complex (MnX)S compounds which have low crystallographic misfit with graphite.[8–10] Typically, an optimized amount of sulfur in the presence of manganese

and other elements such as Fe, Si, Al, Zr, Ti, Ca, and Sr will promote the nucleation of graphite.[11,12]

Sommerfeld and Ton[13] found that the manganese sulfides contained additional elements such as Al, or Mg when small amounts of Mg were added to the melt. The Al compound was identified as Al_2O_3, while the Mg was thought to be part of the sulfide, (MnMg)S. The (MnMg)S particles had the same shape, color, and distribution as the MnS particles. The most efficient type-A graphite nucleation was obtained at a Mn/S ratio of 6.7, but the authors mentioned that the most

Table I. Chemical Composition (Weight Percent) of the Test Samples

Sample no.	CE	C	Si	Mn	P	S	Ti	N	Ti/S	Mn/S
401.1	4.07	3.44	2.07	0.54	0.036	0.120	0.018	0.0037	0.15	4.5
401.5	4.03	3.42	2.02	0.50	0.037	0.120	0.360	0.0033	3	4.2
621.1	4.12	3.51	2.01	0.55	0.015	0.018	0.060	0.0071	3.33	30.6
621.5	4.06	3.45	2.03	0.58	0.015	0.012	0.350	0.0057	29.2	48.3

(a) Sample 401.1 - 0.12%S, 0.018%Ti, Ti/S=0.15

(b) Sample 401.5 - 0.12% S, 0.36% Ti, Ti/S=3

(c) Sample 621.1 – 0.018%S, 0.06%Ti, Ti/S=3.33
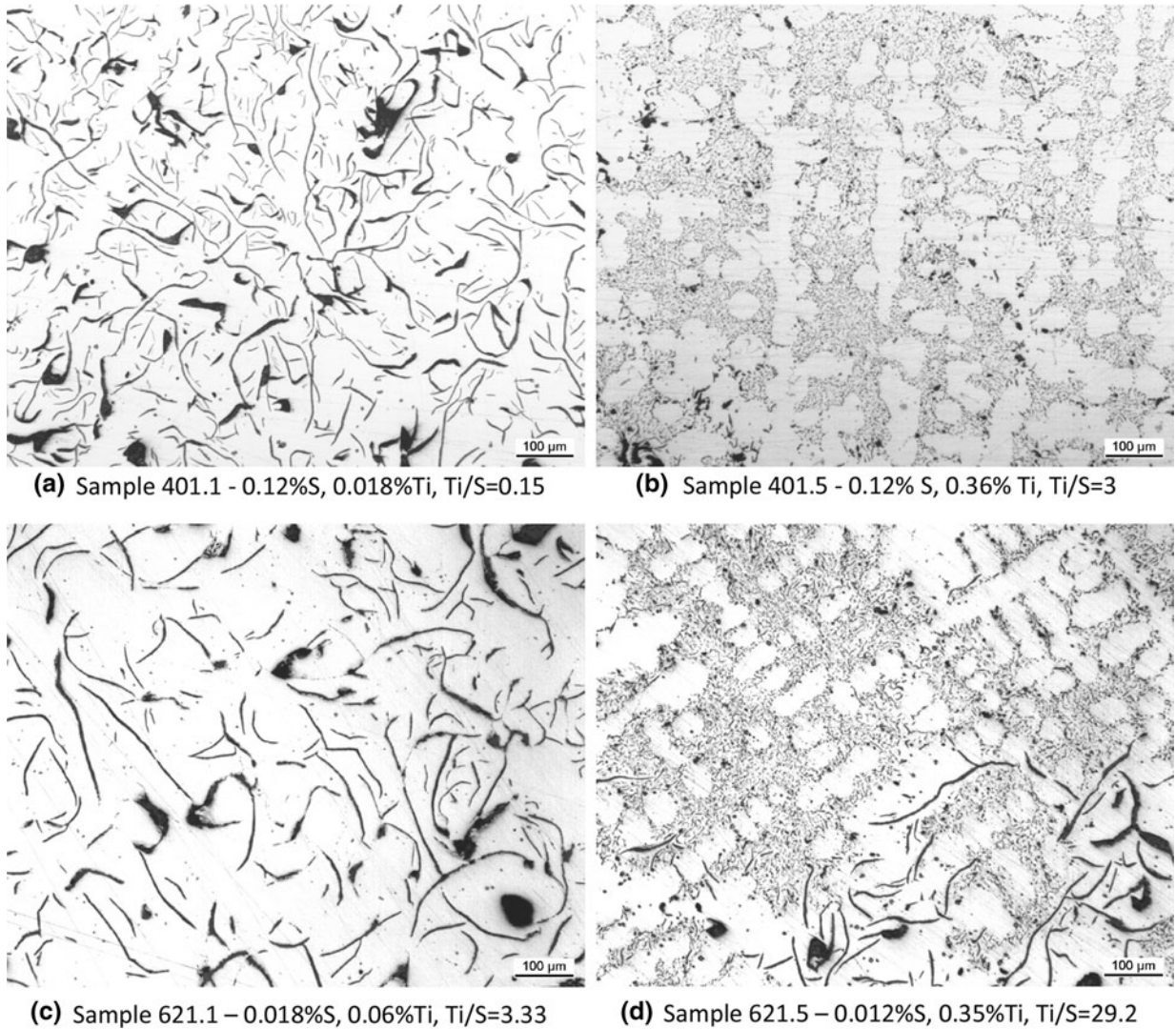
(d) Sample 621.5 – 0.012%S, 0.35%Ti, Ti/S=29.2

Fig. 1—Unetched microstructures: (a) sample 401.1—0.12 pctS, 0.018 pctTi, Ti/S = 0.15; (b) sample 401.5—0.12 pct S, 0.36 pct Ti, Ti/S = 3; (c) sample 621.1—0.018 pctS, 0.06 pctTi, Ti/S = 3.33; (d) sample 621.5—0.012 pctS, 0.35 pctTi, Ti/S = 29.2.

important factor is the Mn- and S-contents and not their ratio. Thermo-Calc simulations suggested that an addition of Al to the melt causes the early [1853 K (1580 °C)] formation of a $SiO_2 \cdot Al_2O_3$ phase, which can serve as nucleant for the MnS sulfides. For a hypoeutectic iron (3.4 pctC, 1.5 pctSi, 0.7 pctMn, 0.05 pctS, 0.04 pctTi) the Thermo-Calc calculation suggested the following sequence of phase formation: austenite at 1468 K (1195 °C), followed by $Ti_4C_2S_2$ at 1458 K (1185 °C), followed by graphite at 1421 K (1148 °C), followed by MnS at 1419 K (1146 °C). Note that this calculation is based on the assumption of thermodynamical equilibrium that ignores kinetic effects. In addition to the sulfides, square-shaped TiN was also observed.

Riposan et al.[14] documented that the additional elements found in the MnS inclusions are usually combined in complex oxides that serve as nuclei for the MnS. The chemistry of the complex oxides and sulfides is based on a large number of factors including the chemistry of the inoculant, of the pre-conditioner, the iron charge and the alloying elements. They proposed that graphite nucleation starts with the precipitation of complex oxides of Al, Si, Zr, Mg, Ti, followed by growth of complex (Mn,X)S sulfides, which constitute the nuclei for flake graphite.

A similar theory of double-layered (cored) nucleation was proposed earlier for spheroidal graphite (SG). Using the results of SEM analysis, Jacobs et al.[15] contended that SG nucleates on duplex sulfide-oxide inclusions (1 μm dia.); the core is made of Ca-Mg or Ca-Mg-Sr sulfides, while the outer shell is made of complex Mg-Al-Si-Ti oxides. This idea was further developed by Skaland and Grong.[10] They argued that SG nuclei are sulfides (MgS, CaS) covered by Mg silicates (e.g., $MgO \cdot SiO_2$) or oxides that have low potency (large disregistry). After inoculation with FeSi that contains another metal (Me) such as Al, Ca, Sr, or Ba, hexagonal silicates ($MeO \cdot SiO_2$ or $MeO \cdot Al_2O_3 \cdot 2SiO_2$) form at the surface of the oxides, with coherent/semi-coherent low energy interfaces between substrate and graphite.

Titanium is well-known to be a deoxidizer and structure refiner in steel. For the case of cast iron, Basutkar et al.[16] argued that titanium additions nucleate dendrites favoring the formation of small equiaxed dendrites. Wallace and co-workers[17,18] found that titanium additions refined the secondary arm spacing in both gray and ductile iron. Ruff and Wallace[19] concluded that the number of austenite dendrites can be increased by reducing the carbon equivalent, adding elements, such as Ti and B, which increase the undercooling by reducing the nucleation potential for graphite or restricting the growth of the eutectic grain, or by adding materials that serve as substrates for austenite nucleation (nitrides, carbonitrides, and carbides of various elements, such as Ti and V). Okada[20] suggested that Ti additions resulting in the formation of TiC, produce low carbon regions at the solid/liquid interface, favoring formation of type-D graphite. Using SEM/
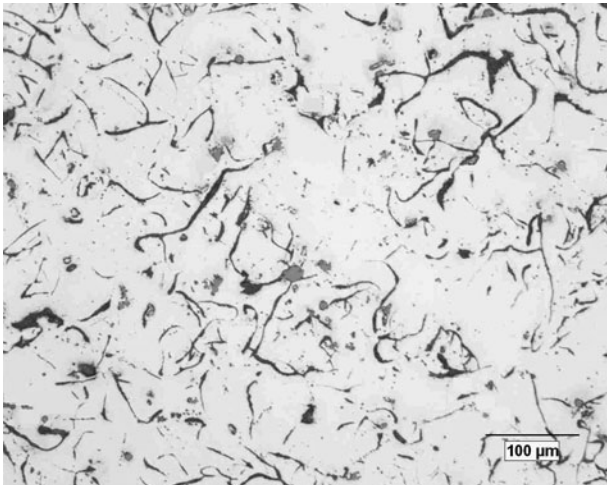
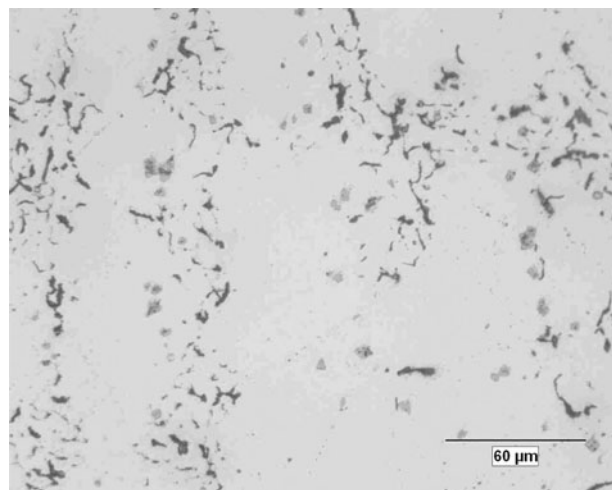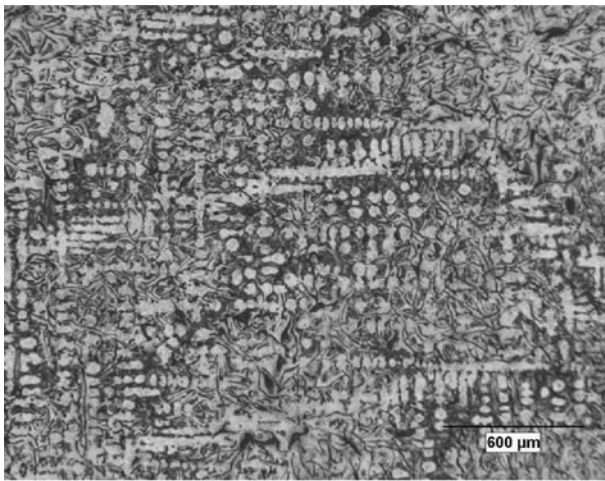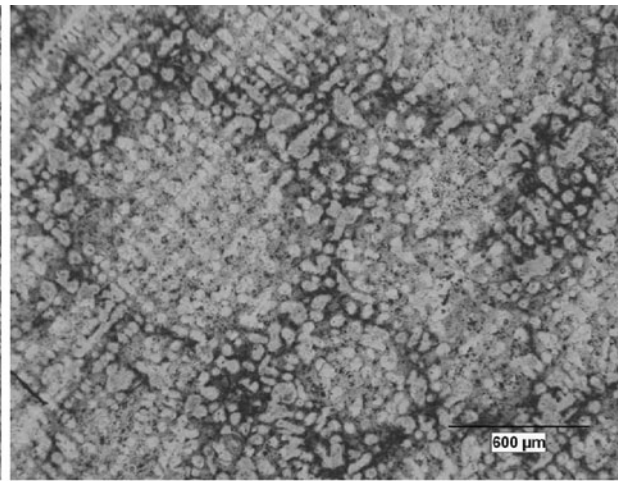(a) 401.1, 0.12%S, 0.018%Ti;
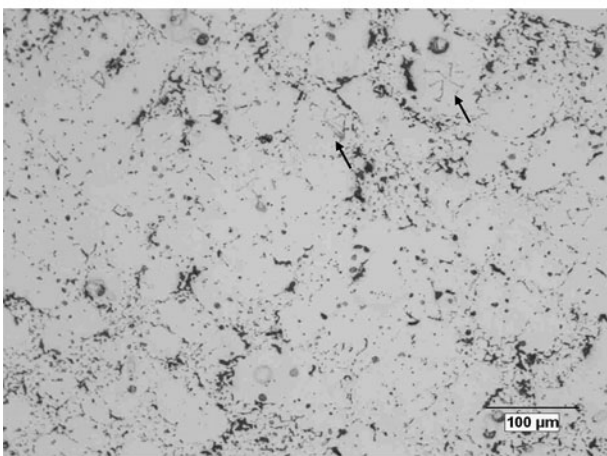
(b) 401.5, 0.12%S, 0.36%Ti

Fig. 2—Microstructure of high-S irons; unetched: (a) 401.1, 0.12 pctS, 0.018 pctTi; (b) 401.5, 0.12 pctS, 0.36 pctTi.

Fig. 3—Microstructure of high-Ti/S sample 621.5—0.012 pctS, 0.35 pctTi; unetched.

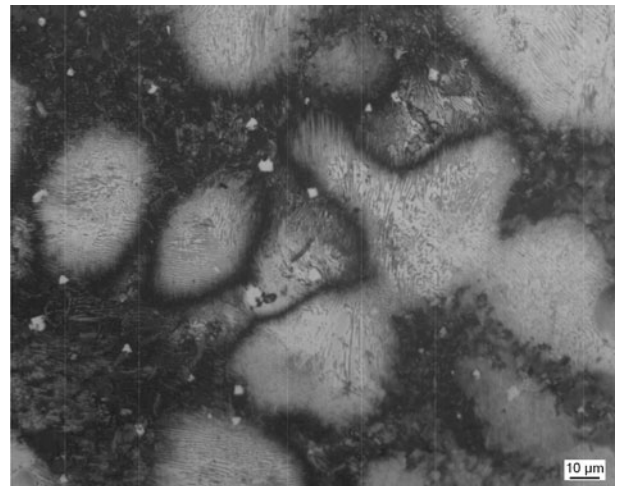**(a) Sample. 401.1 - 0.12%S, 0.018%Ti**
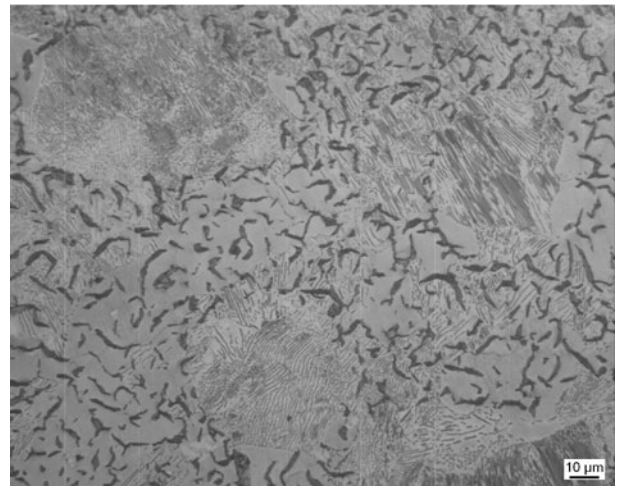

(b) Sample. 401.5 - 0.12%S, 0.36%Ti

Fig. 4—Color-etched micrographs of the high-S irons at low magnification: (*a*) sample. 401.1—0.12 pctS, 0.018 pctTi; (*b*) Sample. 401.5—0.12 pctS, 0.36 pctTi.

Fig. 5—Color-etched micrographs of the sample. 621.1—0.018 pct S, 0.06 pct Ti at high magnification.

(a) inclusions in the interdendritic regions

(b) detail of superfine graphite

EDS analysis, Zeng et al.[21] identified the presence of different Ti compounds in hypoeutectic gray irons containing about 0.08 pctS and up to 0.02 pctTi. The compounds included TiN (35at pctN), (MnTi)S, and TiC. Nakae and Fujimoto[22] identified a graphite type A-to-D transition temperature, $T_{A/D}$, using thermal analysis. Titanium additions increase the $T_{A/D}$ temperature and thus favor type-D graphite formation at smaller undercooling. Yet, no explanation for this behavior was provided.

Wilford and Wilson[23] studied the influence of up to 0.4 pct Ti in gray iron. They stated that first, Ti will react with N producing TiN or Ti(CN) that affects the solidification of primary austenite. The excess Ti will then react with S. Formation of TiS decreases the available S for MnS formation and increases undercooling which is responsible for type-D graphite formation.

Fig. 6—Color-etched micrographs of the sample. 621.5—0.012 pct S, 0.35 pct Ti at high magnification: (*a*) inclusions in the interdendritic regions; (*b*) detail of superfine graphite.
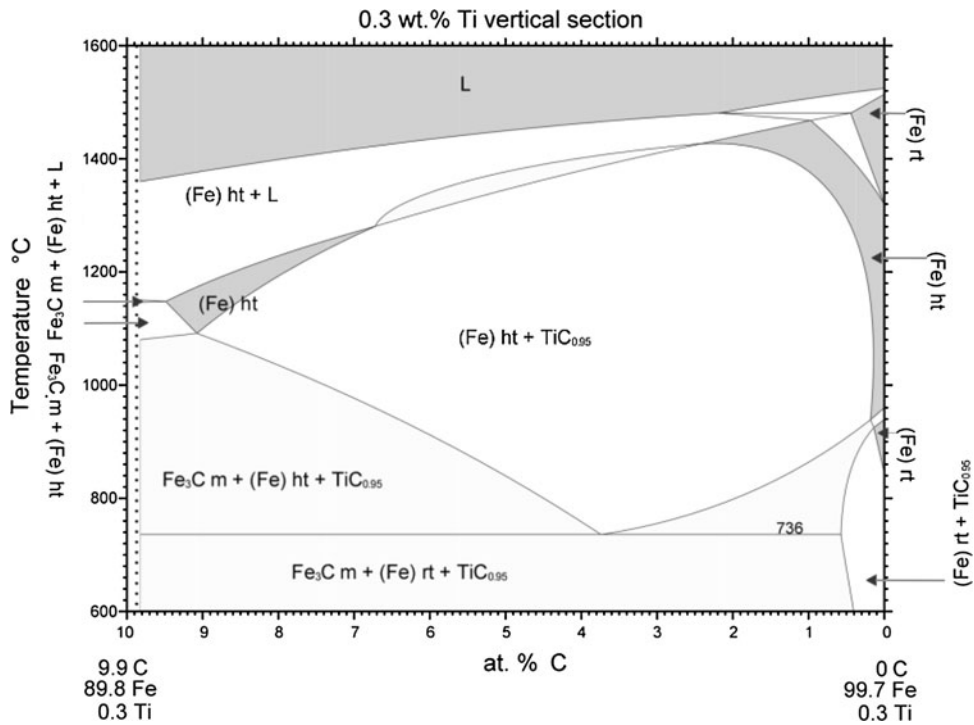
0.3 wt.% Ti vertical section

Fig. 7—Section through the Fe-Ti-C ternary phase diagram.[27]

Table II. Quantitative Metallography Information

| Sample No.	401-1	401-5	621-1	621-5
Graphite Pct Area	10	5.5	10	7.5
Ferrite Pct Area	5	27	8	13

Lux[5] argued that elements of group IV of the periodic table, including Ti and V, form metallic carbides but do not have a nucleation effect, as they do not increase the number of eutectic cells. Sun and Loper[24] also reasoned that, while the atomic structure of TiC is such as to act as nucleus for graphite, the degree of mismatch between the lattices would minimize the nucleation effectiveness of Ti nitrides and carbonitrides. The effect of Ti on graphite shape may not be related to graphite nucleation, but to graphite growth. It is well known that sulfur and oxygen significantly affect graphite shape. According to Park and Verhoven,[25] Scanning Auger Microscopy of fractured graphite surfaces reveals monolayers of S segregated at the iron/graphite interface during solidification. Because of this, S is expected to increase the undercooling required at a given growth rate for both type-A and type-D graphite. Increasing the S level at low Mn contents will result in increased undercooling and finer graphite. It is possible that the effect of Ti is similar to that of S.

This work was undertaken in an attempt to clarify the role of titanium and sulfur in promoting increased fraction of austenite and superfine graphite. A detailed analysis of the graphite through light and electronic microscopy is provided, with particular attention given to the various inclusions that may serve as nuclei for the phases of interest.
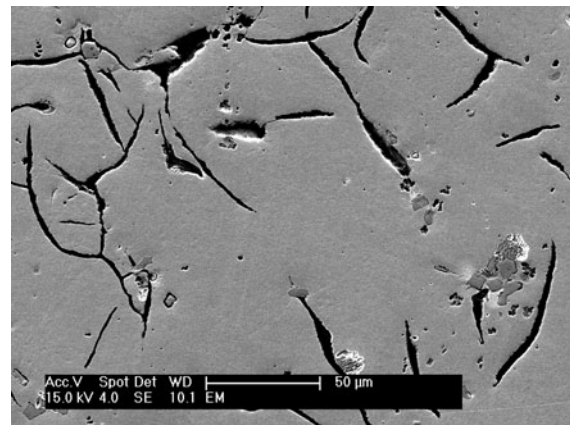
(a) MnS in contact with graphite
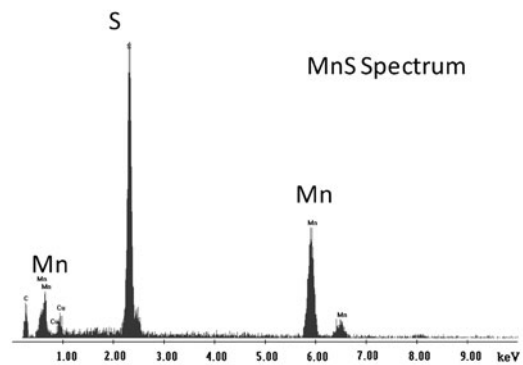
(b) MnS spectrum

Fig. 8—Unetched sample 401.1—0.12 pct S, 0.018 pct Ti; (a) MnS in contact with graphite; (b) MnS spectrum.

II. EXPERIMENTAL PROCEDURE

Two gray iron melts, B401 (high in sulfur) and B621 (low in sulfur), were produced in a medium frequency induction furnace. The complete melting procedure is described in Reference 2. After melt down and superheating at 1773 K (1500 °C), a 50 kg ladle was used to pour iron into two EN-1563 Type II keel blocks (25 mm). An amount of 0.2 pct of a commercial inoculant (chemical analysis: 68.1 pctSi, 0.89 pctAl, 1.65 pctCa, 0.45 pctBi, 0.38 pctBa, and 0.37 pct lanthanides.) was deposited on the bottom of each keel block mold before pouring. The remaining of the iron in the ladle was returned to the furnace. After adjustment of carbon, ferro-titanium (65 pctTi) was added to the melt. The melt was superheated again and a second set of keel blocks was poured.

A detailed metallographic investigation was performed on samples obtained from the keel blocks through both light and electron microscopy. The images have been taken before and after etching.

Some of the samples were color-etched using the etchant: pct25 (80 g) NaOH, 6 pct (20 g) KOH, 6 pct (20 g), picric acid, and (200 mL) 63 pct water. A 2 pctNital was used for deep etching for the SEM analysis. The Leica Qwin Pro software was used for quantitative metallography.

The scanning electron microscopy investigation has been carried out using an XL-30 ESEM FEG (Environmental SEM) (Field Emission Gun) made in 1998 by Philips Electron Optics in conjunction with FEI and Electroscan Corporation. The chemical composition was studied using energy dispersive X-ray spectroscopy (EDX or EDS). The equipment for this was manufactured by Edax. It used a 10 mm^2 "Sapphire" X-ray detector with a "super ultra-thin window" (SUTW), digital pulse processor, and Genesis software. The unetched samples were studied to identify the chemistry of the inclusions and to try to establish a connection between the inclusions and graphite morphology.
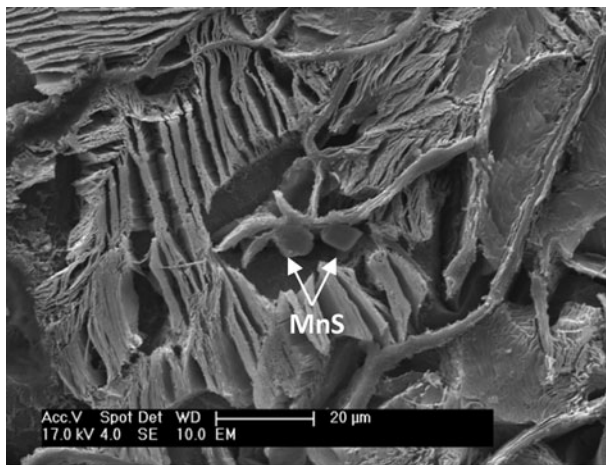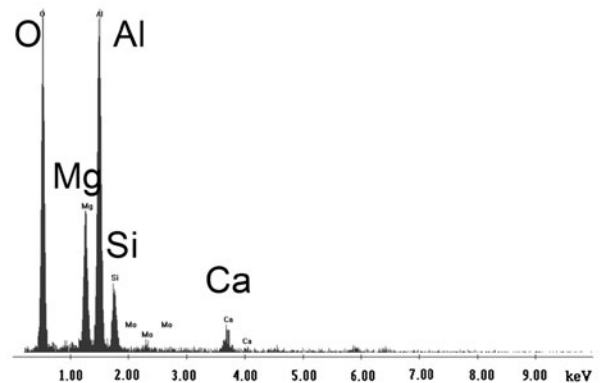

(a) MnS in contact with graphite
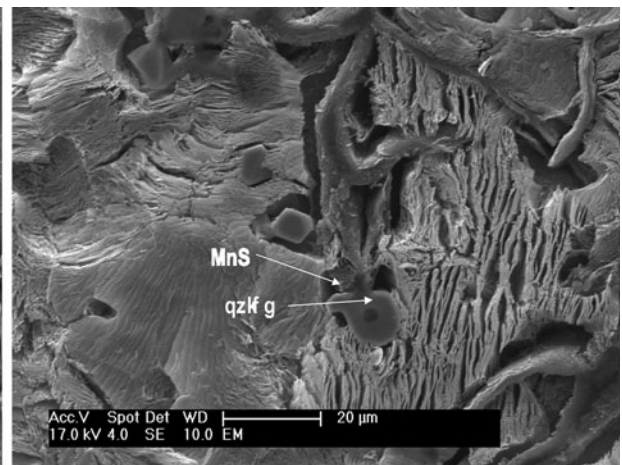
(b) MnS with oxide nucleus
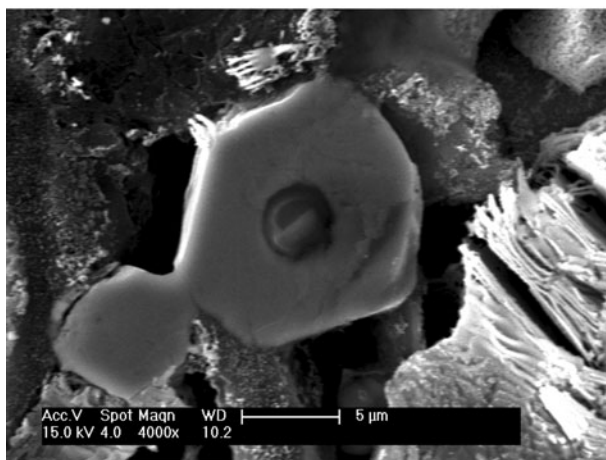
(c) MnS with oxide nucleus (higher magnification);

(d) spectrum of the oxide nucleus

Fig. 9—Sample 401.1—deep-etched with Nital 2 pct: (*a*) MnS in contact with graphite; (*b*) MnS with oxide nucleus; (*c*) MnS with oxide nucleus (higher magnification); (*d*) spectrum of the oxide nucleus.
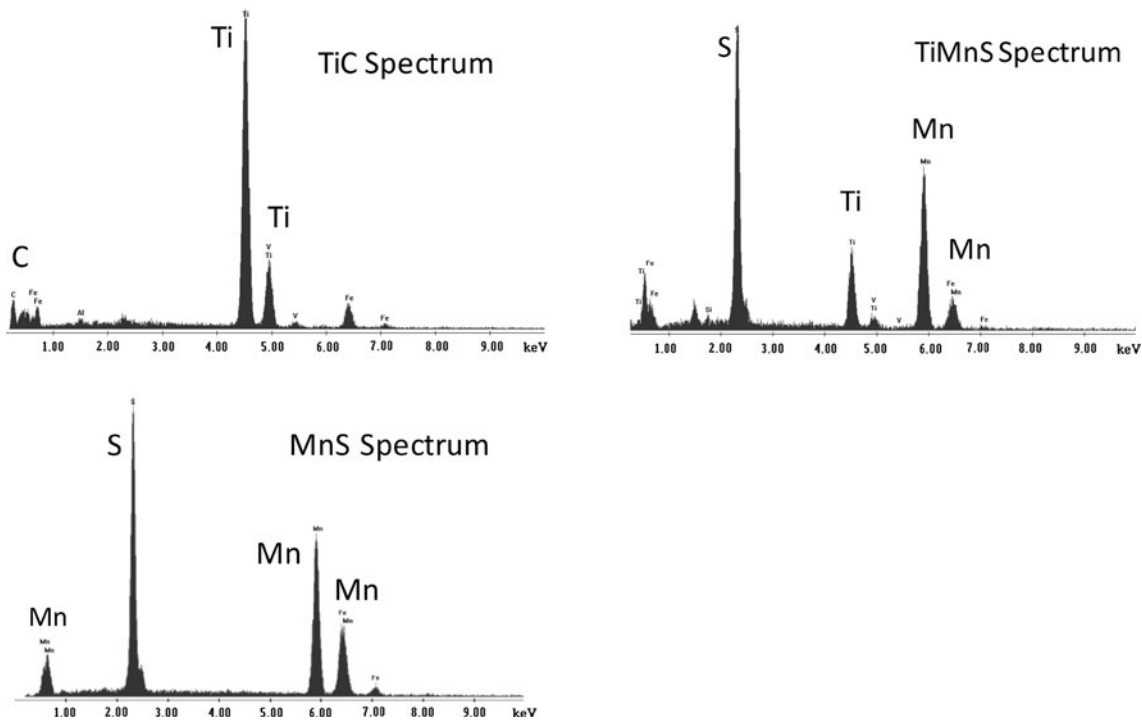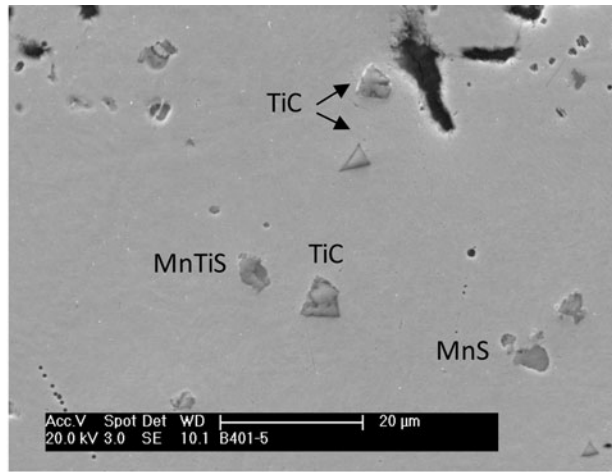
Fig. 10—Unetched sample. 401.5—0.120 pct S, 0.36 pct Ti.

III. RESULTS

The chemical composition of the test samples is given in Table I. The following equation is used to calculate the weight percent of the carbon equivalent:[26]

$$CE = pctC + 0.31 \cdot pctSi - 0.027 \cdot pctMn$$

It can be seen that the compositions of the studied irons are slightly hypoeutectic. The only important difference between the compositions of these irons is the amount of S and Ti. Note that the Ti/S ratio increases from 0.15 to 29.2, and the Mn/S ratio from 4.2 to 48.3. Two of the irons, 401.5 and 621.1 have similar Ti/S ratio, but iron 401.5 has six times more Ti and S than

iron 621.1. Another set of two irons, 401.1 and 401.5, have similar Mn/S ratios, but iron 401.5 has six times more Ti than iron 401.1.

A. Light Microscopy Investigation

The effect of S and Ti on the morphology and size of the graphite is shown in Figure 1. It is seen that the low-Ti irons exhibit in all cases mostly coarse type-A graphite (Figures 1(a) and (c)). Increasing the Ti/S ratio produces finer graphite at the same S level (compare Figures 1(a) and (b), or (c) and (d)). However, a clear difference is seen between the samples having low- or high-S. At the same Ti/S ratio, the
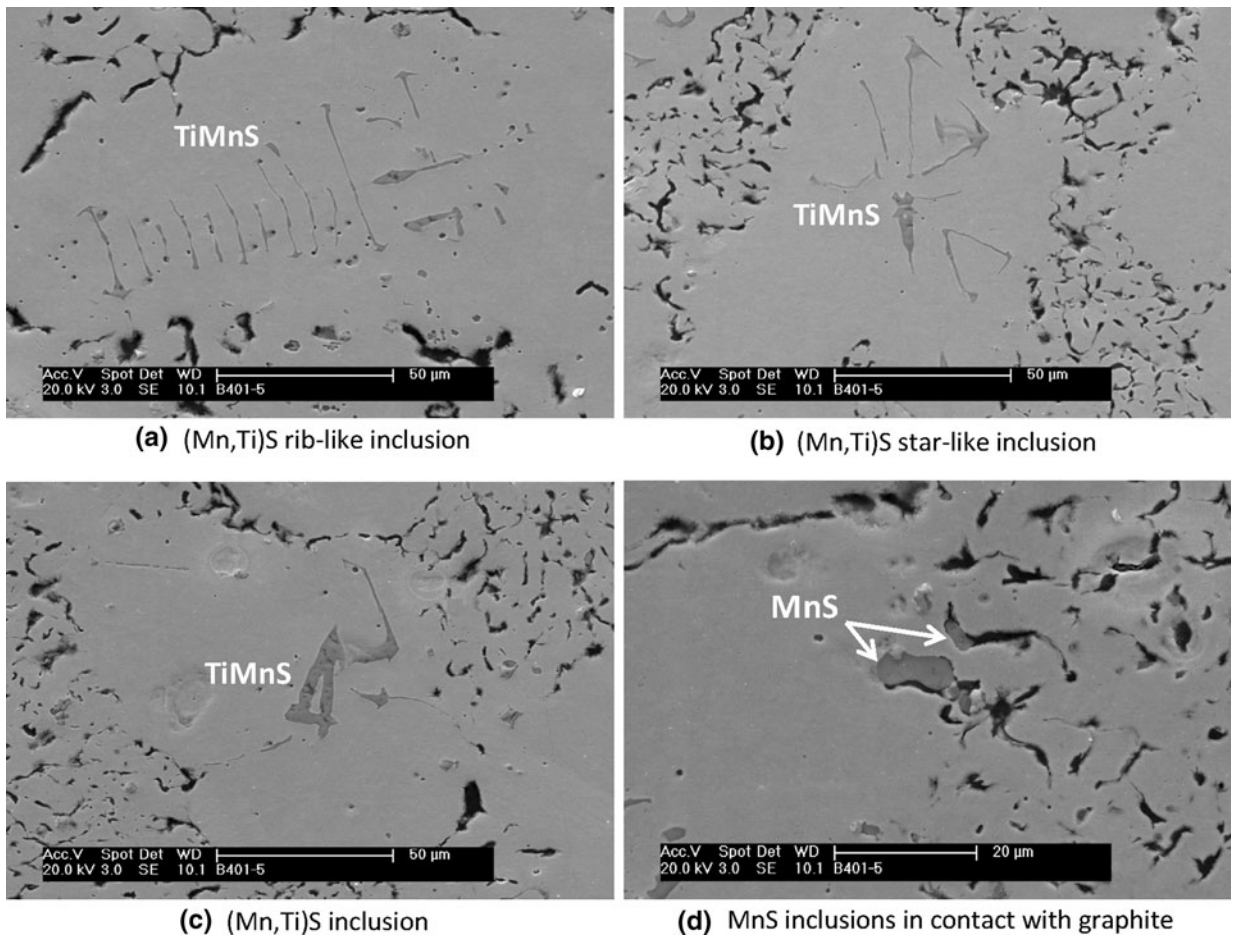
Fig. 11—Unetched SEM micrographs of sample 401.5 showing (Mn,Ti)S and MnS inclusions: (*a*) (Mn,Ti)S rib-like inclusion; (*b*) (Mn,Ti)S star-like inclusion; (*c*) (Mn,Ti)S inclusion; (*d*) MnS inclusions in contact with graphite.

sample with high-S and Ti (401.5) exhibits finer graphite. Indeed, some type-A graphite persist in the microstructure of sample 621.5.

A higher magnification of the high-S iron 401 reveals a large number of inclusions (Figure 2). These inclusions will be identified later through SEM analysis. Titanium addition refines the graphite and also changes the morphology of the inclusions. Indeed, as seen in Figure 2(b), some very large star-like inclusions are noticed in the middle of the secondary arms of the austenite dendrites. These star-like inclusions are not present in the microstructure of the low-S high-Ti irons, as evident from Figure 3. In the low-S high-Ti iron (Ti/ S = 29.2), the inclusions are mostly located at the borders of secondary dendrite arms.

The dramatic effect of high-Ti/S ratio on the microstructure is clearly illustrated in Figure 4 for the case of the high-S irons. Larger eutectic grains and less oriented dendrites are noticed.

The high magnification colored micrograph of low-Ti/ S ratio low-S iron in Figure 5 shows few inclusions, one TiC and one MnS. The Ti carbide is in the middle of the matrix, while the Mn sulfide is attached to a graphite flake.

Increasing the Ti/S ratio in the low-S iron, raises manifold the number of inclusions. In Figure 6(a), it is seen that the inclusions are pushed by the growing dendrites in the last regions to solidify. In an earlier report[1], it was shown that the fraction of primary austenite in the high-S iron 401.5 increased from 0.17 to 0.27 as the Ti/S ratio increased (Ti increased from 0.018 to 0.36 pct). However, titanium carbides do not seem to act as nuclei for the austenite since they are positioned in the interdendritic regions.

The picture on Figure 6(b) presents a detail of the superfine graphite. It is short and stubby with a typical length of 10 to 20 μm.

According to the ternary phase diagram of Fe-C-Ti presented in Figure 7, for a 3.5 pctC iron, TiC can precipitate at temperatures considerably higher than the liquidus of cast iron. Thus, it is reasonable to assume that Ti carbides forms in the liquid, before the beginning of the austenite solidification, and are pushed in the last regions to solidify by the austenite dendrites.

Quantitative metallographic information is provided in Table II. It is seen that Ti additions reduce the amount of graphite and increase the amount of ferrite.
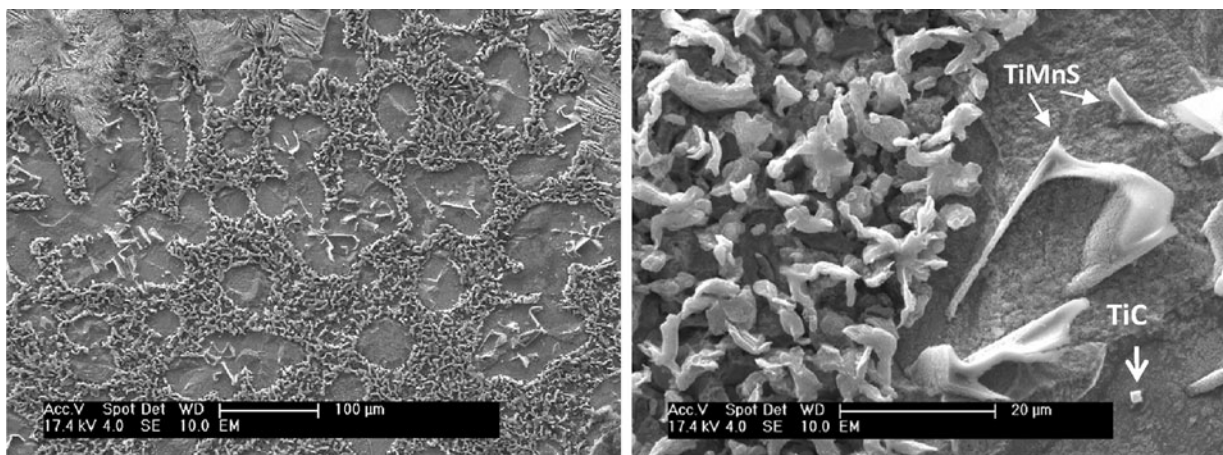
(a) (MnTi)S inclusions in the austenite dendrites

(b) (MnTi)S inclusions in austenite (higher magnification)
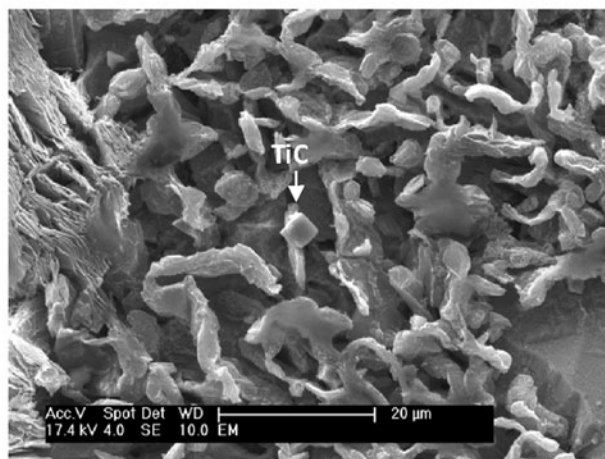
(c) Superfine graphite and TiC

Fig. 12—Deep-etched micrographs of sample 401.5—0.120 pctS, 0.36 pctTi: (*a*) (MnTi)S inclusions in the austenite dendrites; (*b*) (MnTi)S inclusions in austenite (higher magnification); (*c*) superfine graphite and TiC.

The higher ferrite content is the result of decreased carbon diffusion distances because of the finer graphite.

### B. Scanning Electron Microscopy (SEM) Investigation

In the high-S low-Ti iron (B401.1), a large number of polygonal MnS inclusions were found (Figure 8). More than 50 pct of these inclusions seem to be attached to the sides of the graphite flakes (Figure 9(a)). Complex Al-Mg-Si-Ca oxide compounds were identified at the center of some of the MnS particles (Figures 9(b) through (d)).

In the presence of both Ti and S (sample B401.5) a variety of inclusions with different morphologies was found. The smaller inclusions and their spectrum are shown in Figure 10. The majority of the inclusions in this sample are (MnTi)S, with a variety of morphologies (Figure 11). As also shown in Figure 2(b), the (MnTi)S inclusions are mostly formed in the middle of the dendrites. It is reasonable to assume that they have

acted as nuclei for the austenite dendrites. This would explain the significant increase in the fraction of austenite as the Ti/S ratio increased from 0.15 to 3. MnS inclusions were also found in this iron (Figure 11(d)), and again, they seemed to act as nuclei for the graphite.

Deep-etched microstructures of sample B401.5 (Ti/ S = 3) are shown in the Figure 12. The presence of (MnTi)S inclusions in the austenite is confirmed (Figures 12(a) and (b)). It is the dominant inclusion. A few TiC inclusions were found in the austenite (Figures 12(a) and (b)), and many TiC inclusions were found in the proximity of the superfine graphite flakes (Figure 12(c)). Yet, as they do not show clear contact with graphite (they always seem to be on top and not on the side of the graphite), in our opinion, the appearance is not that of graphite nuclei.
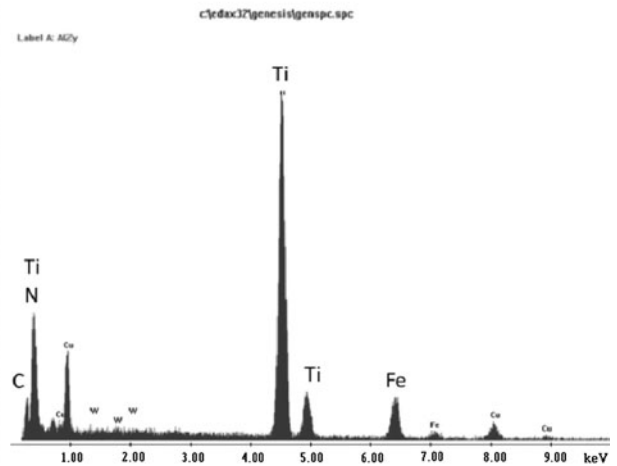
The images of the deep-etched sample B621.1 (low-S low-Ti, medium Ti/S ratio) are presented in Figure 13. The microstructure exhibits coarse type-A graphite (length 100 to 200 μm) and almost no inclusions (Figure 13(a)). This sample exhibited very few
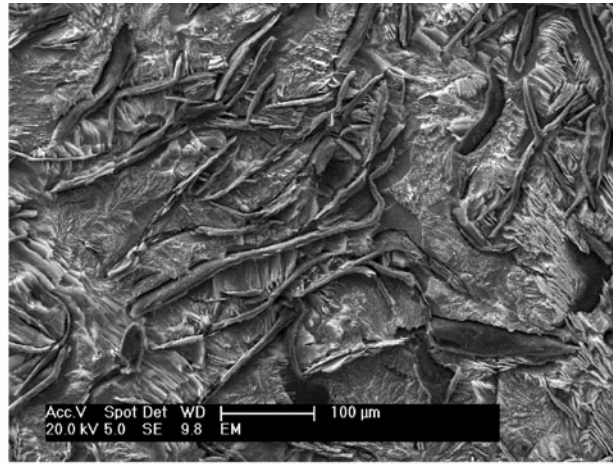
(a) coarse type-A graphite
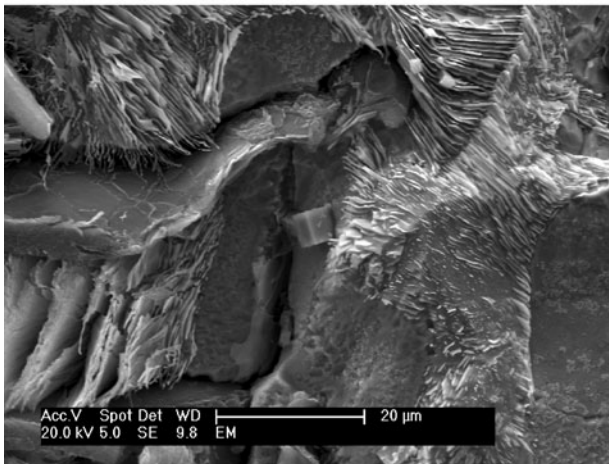
(b) Ti carbonitride

(c) spectrum of the carbonitride

Fig. 13—Deep-etched micrographs of sample 621.1—0.018 pctS, 0.06 pctTi: (*a*) coarse type-A graphite; (*b*) Ti carbonitride; (*c*) spectrum of the carbonitride.

inclusions. The spectrum of the cubic inclusions found indicates the composition of a titanium carbonitride Ti(NC). While the pick of Ti and N are at the same keV, this pick was very small in other TiC spectra.

A dramatic change in the microstructure occurs when the Ti/S ratio is raised to 29.2 for sample 621.5 with low-S high-Ti (0.012 pctS, 0.35 pctTi). A large number of cubic TiC particles are observed (Figure 14(a)). This is consistent with previous research[1] where it was found that the number of Ti compounds increases significantly as the Ti content in the iron increases. They are the dominant inclusions at this composition. As also documented earlier in this report, the TiC particles are pushed by the austenite dendrites to the last regions to solidify (Figure 14(a)). There is no evidence to show that TiC could act as nuclei for the primary austenite. However, isolated

instances where the TiC is in contact with the graphite have been found (Figure 14(c)). We do not feel that this is enough proof to demonstrate a graphite nucleation effect by the TiC. A few MnS inclusions in contact with the graphite were also observed (Figure 14(b)). The graphite flakes are thick and short (Figures 14(c) and (d)).

A summary of the type and location of inclusions as a function of composition and the Ti/S ratio is given in Table III. Note again that the amount of inclusions in the low-S low-Ti sample (621.1) was minimal.

Some high magnification pictures of the superfine graphite are presented in Figure 15. It is seen that the graphite flakes are very short, thick, and that they bend and twist significantly. While most of the growth is along the A-direction, in some instances growth in the C-direction appears to occur (Figure 15(b)). The
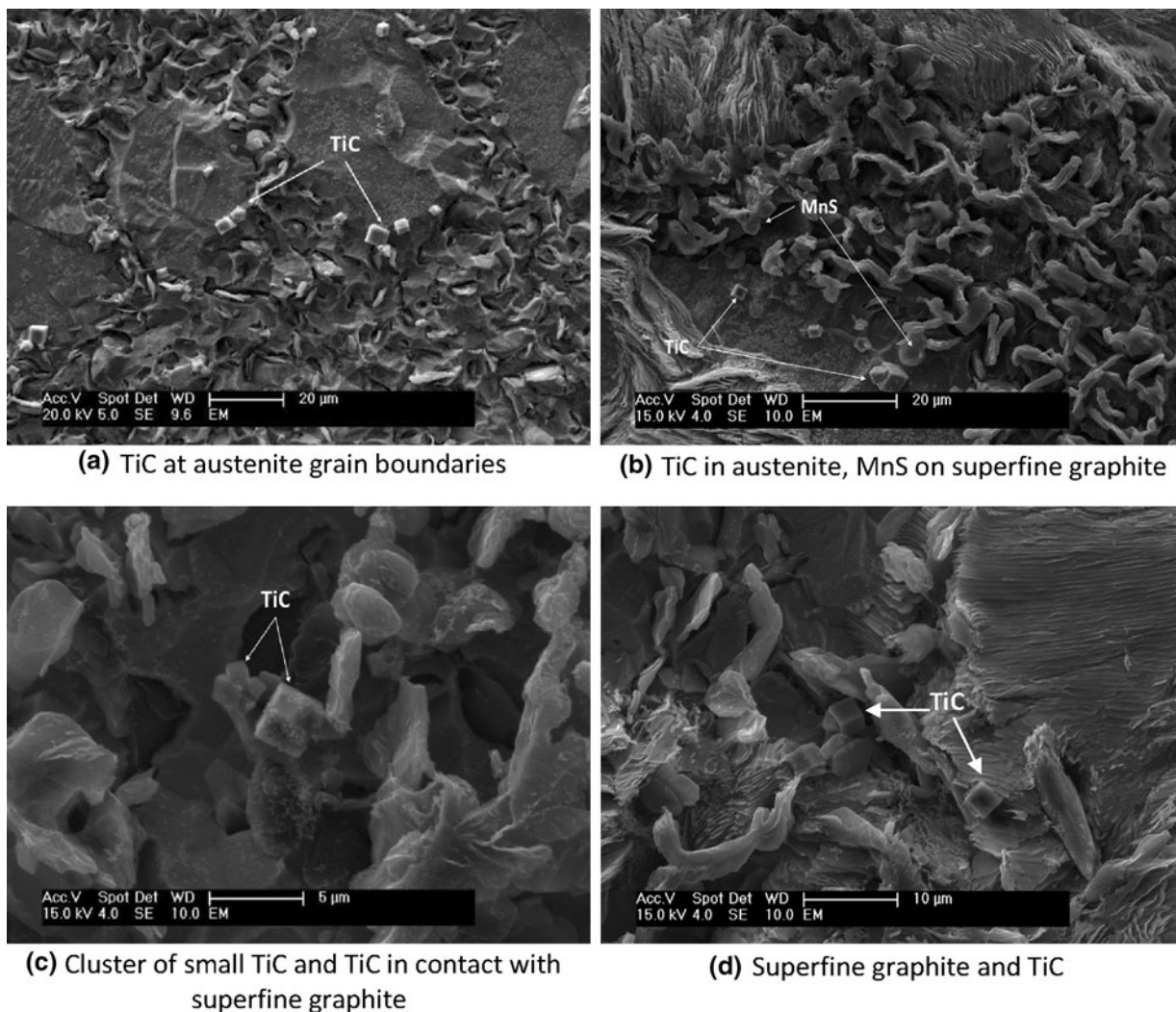
(a) TiC at austenite grain boundaries

(b) TiC in austenite, MnS on superfine graphite

(c) Cluster of small TiC and TiC in contact with superfine graphite

(d) Superfine graphite and TiC

Fig. 14—Deep-etched micrographs of sample 621.5—0.012 pctS, 0.35 pctTi: (*a*) TiC at austenite grain boundaries; (*b*) TiC in austenite, MnS on superfine graphite; (*c*) cluster of small TiC and TiC in contact with superfine graphite; (*d*) superfine graphite and TiC.

graphite branch growing in the C-direction shows an exposed hexagonal plane and is very similar to the corral graphite. A more detailed analysis is required to support this statement.

IV. DISCUSSION

There are two major effects of the Ti additions that need to be understood: the increased amount of austenite and the formation of the superfine interdendritic graphite. Arguments involving nucleation and growth kinetics of the phases must be considered.

As shown in Table IV, Ti addition to both low- and high-S irons results in an increase of the liquidus temperature, TL, and a decrease of the minimum eutectic temperature, TE_{min}. The classic explanation for the first effect is an increase in the nucleation potential. Indeed, the Ti addition to a melt with sufficient S (401.5—0.12 pctS), produces complex (MnTi)S that are nucleation sites for austenite but not for graphite. As formation of (MnTi)S depletes the melt from sulfur, less S is available for the precipitation of MnS inclusions that are the main nucleant for type-A graphite. This results in the depression of the eutectic temperature. Thus, for high-S iron, Ti additions will increase the amount of austenite through enhanced austenite nucleation and increased liquidus-eutectic interval, which allows more time for austenite growth before the eutectic reaction. A higher amount of dendritic austenite will favor a type-A to type-D transition for graphite, as the graphite is constrained
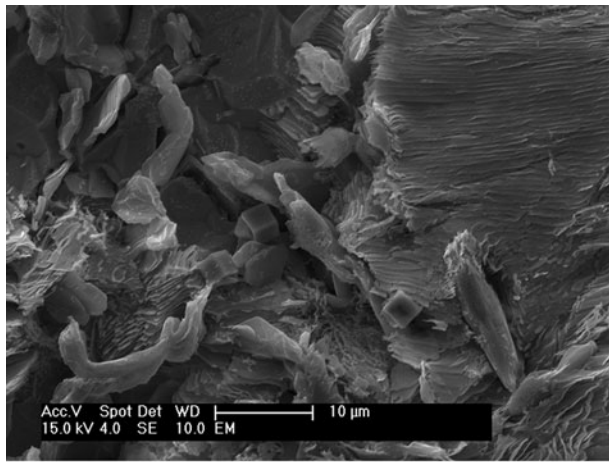
(a) superfine graphite
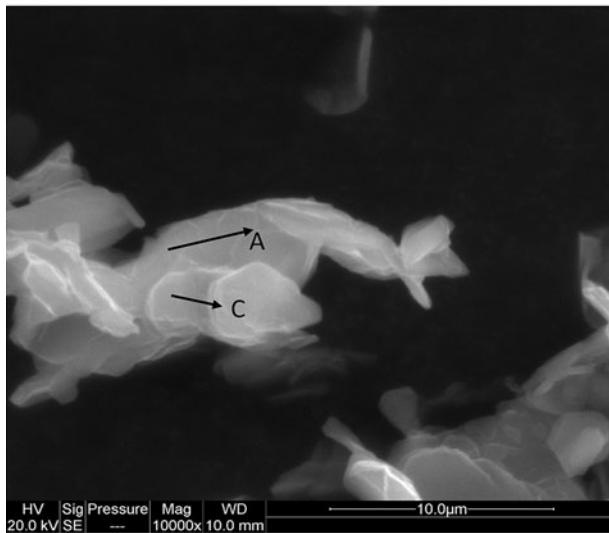
(b) growth in A- and C-direction

Fig. 15—SEM micrographs of superfine graphite from deep-etched sample 621.5: (*a*) superfine graphite; (*b*) growth in A- and C-direction.

to grow between the dendrite arms. Titanium absorption on the graphite plates could also interfere with graphite growth, similar to the mechanism described by Park and Verhoven[25] for sulfur.

For the low S irons, the situation is less clear. While the higher amount of austenite produced by Ti additions can still be attributed to the higher liquidus-eutectic interval (Table III), the reasons for the increase remain partially unexplained. The probable explanation for the higher liquidus is increased nucleation. Yet, we were not able to identify nucleation sites for the austenite in iron 621.5. The higher TE_{min} in the absence of Ti, and the highest TE_{min} for the highest purity iron from the series (621.5) can be understood through equilibrium thermodynamics. Indeed, low-S and Ti content decrease the stable eutectic temperature by similar amounts (Table III page 65 in Reference 26) and thus, purer irons should have higher eutectic equilibrium temperature. The kinetic effect of Ti absorption on the graphite will also act in the same direction and is probably responsible for the formation of the superfine graphite.

The fact that Ti addition produced larger eutectic cells supports the theory that Ti is not producing finer graphite because of a change in the nucleation potential, but because of lower growth rate of the graphite in between the dendrite arms of a larger fraction of austenite.

Table IV. Thermal Analysis Data and Fraction of Austenite

Sample No.	TL [K (°C)]	TE_{min} [K (°C)]	TL − TE_{min} [K (°C)]	Austenite Fraction
401.1	1455 (1182)	1420 (1147)	308 (35)	0.17
401.5	1465 (1192)	1418 (1145)	320 (47)	0.27
621.1	1460 (1187)	1421 (1148)	312 (39)	0.27
621.5	1471 (1198)	1417 (1144)	327 (54)	0.38

Table III. Summary of Types and Location of Inclusions From SEM Analysis

Sample	pctS	pctTi	Ti/S	Mn/S	Graphite	Dominant Inclusion	Inclusion Location	Other Inclusions
401.1	0.12	0.018	0.15	4.5	type-A	MnS	in contact with Gr	none
401.5	0.12	0.36	3	4.2	interdendritic/superfine	(Mn,Ti)S	in austenite	MnS, TiC
621.1	0.018	0.06	3.33	30.6	type-A	TiC, Ti(CN)	in austenite	MnS
621.5	0.012	0.35	29.2	48.3	superfine + some type A	TiC	at austenite grain boundaries; in contact with graphite (?)	MnS

V. CONCLUSIONS

It was confirmed that when sufficient sulfur is present in the iron nucleation occurs on Mn sulfides that have a core of complex Al, Ca, Mg oxide. Both type-A and type-D graphite were observed to grow on the Mn sulfide. An increased titanium level of 0.35 pct produced superfine interdendritic graphite (~10 μm) at low as well as at high-S contents. The shape of the graphite was also dramatically altered. Ti also produced larger eutectic grains (cells).

While TiC additions increased the liquidus temperature, TiC did not appear to be a nucleation site for the primary austenite in low sulfur iron as it was found mostly at the periphery of the secondary arms of the austenite, in the last region to solidify. The effect of titanium in refining the graphite and increasing the austenite fraction can be explained through the widening of the liquidus-eutectic temperature interval (more time for austenite growth) and the decrease in the growth rate of the graphite.

In the presence of high-Ti and S, (MnTi)S star-like and rib-like inclusions were found in the middle of the austenite dendrites. It is reasonable to assume that they are acting as nuclei for the austenite.

ACKNOWLEDGMENTS

REFERENCES

1. P. Larrañaga, J. Sertucha, A. Loizaga, R. Suárez, and D.M. Stefanescu: *Trans. AFS,* 2012, vol. 120, pp. 337–46.
2. P. Larrañaga, J. Sertucha, A. Loizaga, R. Suárez, and D.M. Stefanescu: *Trans. AFS,* 2012, vol. 120, pp. 347–53.
3. B. Lux and H. Tannenberger: *Mod. Cast.*, 1962, vol. 41, p. 57.
4. D.M. Stefanescu: *Giesserei-Praxis*, 1972, vol. 24, p. 430.
5. B. Lux: in *Recent Research on Cast Iron*, H. D. Merchant, ed., Gordon and Breach, New York, NY, l968, p. 241.
6. W. Weis: in *The Metallurgy of Cast Iron*, B. Lux, I. Minkoff and F. Mollard eds., Georgi Publishing Co., St Saphorin, 1974, pp. 69–79.
7. J.F. Wallace: *Trans. AFS*, 1975, vol. 83, p. 373.
8. L.R. De and Y.J. Xiang: *Trans. AFS*, 1991, vol. 99, pp. 707–12.
9. M. Chisamera, I. Riposan, and M. Barstow: *AFS Int. Inoculation Conf.*, Rosemont, IL. 1998. Paper 3.
10. T. Skaland, F. Grong, and T. Grong: *Metall. Trans.*, 1993, vol. 24A, 2321p. and 2347p.
11. K. Muzumdar and J. Wallace: *Trans. AFS*, 1973, vol. 81, pp. 412–23.
12. I. Riposan, M. Chisamera, S. Stan, and T. Skaland: *Proc. AFS Cast Iron Inoculation Conf.* 2005. pp. 31–41.
13. A. Sommerfeld and B. Tonn: in *The Carl Loper Cast Iron Sympos.*, Madison, WI. 2009. pp. 168–78.
14. I. Riposan, M. Chisamera, S. Stan, C. Hartung, and D. White: in *The Carl Loper Cast Iron Sympos.,* Madison, WI. 2009. pp. 191–200.
15. M.M. Jacobs, T.J. Law, D.A. Melford, and M.J. Stowell: *Met. Technol.*, 1974, vol. 1, p. 490.
16. P. Basutkar, S. Yew, and C. Loper: *Trans. AFS*, 1969, vol. 77, pp. 321–28.
17. J.F. Wallace: *Trans. AFS*, 1975, vol. 83, pp. 363–78.
18. R. Naro and J.F. Wallace: *Trans. AFS*, 1969, vol. 77, pp. 311–20.
19. G. Ruff and J.F. Wallace: *Trans. AFS*, 1976, vol. 84, pp. 705–28.
20. A. Okada and H. Miyake: *The Unknown World of Cast Iron*, KANSAI University Press, Osaka, 1996, p. 141.
21. D. Zeng, Y. Zhang, J. Liu, H. He, and X. Hong: in *Science and Processing of Cast Iron VIII*, Y. Li *et al.* eds., Tsinghua University Press, 2006, pp. 86–91.
22. H. Nakae and K. Fujimoto: *Key Eng. Mater.*, 2011, vol. 457, pp. 25–30.
23. K.B. Wilford and F.G. Wilson: *Br. Foundrym.*, 1985, vol. 75, 301p. and 364p.
24. G.X. Sun and C.R. Loper: *Trans. AFS*, 1983, vol. 91, pp. 639–46.
25. J.S. Park and J.D. Verhoven: *Metall. Mater. Trans. A*, 1996, vol. 27A, pp. 2740–53.
26. D.M. Stefanescu: *Metals Handbook*, 9th ed., ASM International, Materials Park, OH, 1988, vol. 15, pp. 61–70.
27. H. Ohtani, T. Tanaka, M. Hasebe, and T. Nishizawa: *CALPHAD*, 1988, vol. 12, pp. 225–46.